

RHEINISCHE FRIEDRICH-WILHELMS-UNIVERSITÄT BONN

ADVANCED LABORATORY COURSE

E106: Cavities

Authors

Paarth Thakkar
Keito Watanabe

Head Tutor

Dr. Michael Switka

April 4, 2022

Contents

1	Introduction	2
2	Theoretical Background	3
2.1	Waveguides	3
2.1.1	Cylindrical waveguides	4
2.1.2	Cylindrical waveguides resonator	4
2.2	Oscillating circuit	5
2.2.1	Quality factor	6
2.2.2	Coupling coefficient	6
2.2.3	Reflection coefficient	6
2.2.4	Shunt impedance	7
2.3	Scalar measurement of reflection coefficient	7
2.4	Vectorial measurement of reflection coefficient	8
2.4.1	Determining resonant frequency and coupling	9
2.4.2	Determining quality factor	10
2.5	Bead pull measurement	10
2.5.1	Resonant bead pull measurement	10
2.5.2	Non-resonant bead pull measurement	10
2.5.3	Shunt impedance	11
2.6	What is dB?	11
2.7	What is dBm?	11
2.8	Exercise before the experiment	11
3	Experimental Setup	12
3.1	Procedure	12
3.1.1	Attenuation and Reflection in Coaxial Cables	12
3.1.2	Scalar Measurement	14
3.1.3	Vectorial Measurement	15
3.1.4	Bead-Pull Measurement	15
3.2	Results	17
3.2.1	Attenuation of Coaxial Cables	17
3.2.2	Scalar Measurement	17

Chapter 1

Introduction

As the title might suggest, in this experiment we will be studying cavities. Before talking about cavities themselves though, it is important to understand why we are studying them. Cavity resonators are important optical and microwave system components [1]. The main principle is that it has constructive and destructive interference pattern inside and enclosed region. They can be used as a filters, or as antennas or in lasers. They also have a wide range of application in particle accelerators [2].

Chapter 2

Theoretical Background

2.1 Waveguides

In order to understand cavities, we start off with the discussion on waveguides. An electromagnetic wave, when confined to the interior of a hollow pipe is called a waveguide. We shall closely follow the laboratory script [3] for our report. The generalized Maxwell equations in terms of E-field and H-field are given by:

$$\nabla \times \mathbf{E} = -\frac{\partial \mathbf{B}}{\partial t} \quad (2.1.1)$$

$$\nabla \cdot \mathbf{D} = \rho \quad (2.1.2)$$

$$\nabla \times \mathbf{H} = \vec{j} + \frac{\partial \mathbf{D}}{\partial t} \quad (2.1.3)$$

$$\nabla \cdot \mathbf{B} = 0 \quad (2.1.4)$$

In vacuum, these equations become:

$$\nabla \times \mathbf{E} = \mu_0 \cdot \frac{\partial \mathbf{H}}{\partial t} \quad (2.1.5)$$

$$\nabla \cdot \mathbf{E} = 0 \quad (2.1.6)$$

$$\nabla \times \mathbf{H} = \epsilon_0 \cdot \frac{\partial \mathbf{E}}{\partial t} \quad (2.1.7)$$

$$\nabla \cdot \mathbf{H} = 0 \quad (2.1.8)$$

Upon solving these equations, we get plane wave solutions which looks like this:

$$\Delta \vec{E}(\vec{r}) + \frac{\omega}{c^2} \vec{E}(\vec{r}) = 0$$

$$\Delta \vec{B}(\vec{r}) + \frac{\omega}{c^2} \vec{B}(\vec{r}) = 0$$

Now, let us look at a waveguide which is aligned along the z-direction. Taking the ansatz $\vec{E} = \vec{E}(x, y) e^{i(\omega t - kz)}$ and the separation $\Delta = \Delta_{\perp} + \frac{\partial^2}{\partial z^2}$, for the longitudinal fields yields:

$$\Delta_{\perp} E_z + k_c^2 E_z = 0 \quad (2.1.9)$$

$$\Delta_{\perp} H_z + k_c^2 H_z = 0 \quad (2.1.10)$$

where

$$k_c^2 = \frac{\omega^2}{c^2} - k^2$$

The quantity k_c is called the critical wave number and is a characteristic property of the cavity, as we shall see. Solving these equations further, we see that it is sufficient to know the longitudinal fields, E_z and B_z because we can easily determine the transverse components from them.

$$ik_c^2 \vec{E}_{\perp} = k \vec{\nabla}_{\perp} E_z + \omega \mu_0 \vec{\nabla}_{\perp} H_z \times \hat{e}_z \quad (2.1.11)$$

$$ik_c^2 \vec{H}_{\perp} = k \vec{\nabla}_{\perp} H_z - \omega \epsilon_0 \vec{\nabla}_{\perp} E_z \times \hat{e}_z \quad (2.1.12)$$

Now, there are two waves to classify these waves:

1. $k_c^2 = 0$
 - (a) $\vec{\Delta}_\perp E_z \neq 0$ and $\vec{\Delta}_\perp H_z \neq 0$: HE or EH hybrid waves.
 - (b) $\vec{\Delta}_\perp E_z = 0$ and $\vec{\Delta}_\perp H_z = 0$: TEM waves.
2. $k_c^2 \neq 0$ In this case we do not get any propagation if $\omega \leq c \cdot k_c$. These waves are called evanescent waves or the cut off condition. The possible propagation modes are:
 - (a) $E_z = 0$: TE (transversal electric) or H waves.
 - (b) $H_z = 0$: TM (transversal magnetic) or E waves.

Corresponding to this critical wave, we have a critical frequency, which is $\omega_c = k_c \cdot c$, below which there is no propagation. One interesting thing to note here is that for a hollow waveguide, only TE or TM modes are possible, TEM is not, because no wave would exist in this case [4]. But for a coaxial cable, which consists of straight wire surrounded by a conduction sheath, we can get TEM modes.

2.1.1 Cylindrical waveguides

We now consider a cylindrical waveguide with an inner radius a . This imposes the following boundary conditions to the walls of the waveguide:

- $E_\phi = 0, E_z = 0$ for $r = a$
- $H_r = 0$ for $r = a$

The field distribution solution for a cylindrical waveguide can be separated into angular and radial parts, whose solutions are then given by the Bessel/Neumann functions. These can be then substituted in the eq.(2.1.11)-(2.1.12) and upon imposing the constraints from the boundary condition gives us the corresponding TE- and TM-modes.

2.1.2 Cylindrical waveguides resonator

The time has now come, to talk about cavities itself. If we now insert two conducting plates perpendicular to the z-axis, the incoming wave is reflected completely, giving us standing waves. Because of this, the z-dependence changes like:

$$a \cdot e^{ikz} \implies A \cdot \sin(kz + \phi_0)$$

The following condition is imposed so that the longitudinal boundary conditions are fulfilled: $k = p \cdot \pi/l$. The longitudinal field looks like:

$$\begin{aligned} \textbf{TE}_{mnp} - \textbf{Modes} : H_z &= H_{mn} \cdot J_m(k_c r) \cos(m\phi) \cdot \sin(p\pi/l \cdot z) \cdot e^{\omega_{mnp} t}; \\ &\text{where } k_c a = j'_{mn} \\ \textbf{TM}_{mnp} - \textbf{Modes} : E_z &= E_{mn} \cdot J'_m(k_c r) \cos(m\phi) \cdot \cos(p\pi/l \cdot z) \cdot e^{\omega_{mnp} t}; \\ &\text{where } k_c a = j_{mn} \end{aligned}$$

For resonant frequency, we have:

$$\omega_{mnp} = c \cdot \sqrt{(j_{mn}/a)^2 + (p\pi/l)^2}$$

Here, J_m is the m -th Bessel function, J'_m is its derivative. And j_{mn} and j'_{mn} are the n -th zeropoints of the m -th Bessel function and its derivative.

The resonant modes can be written in the linear form as:

$$(d\nu)^2 = \left(\frac{c j'_{mn}}{\pi} \right)^2 + \left(\frac{c}{2} \right)^2 p^2 \left(\frac{d}{l} \right)^2 \quad (2.1.13)$$

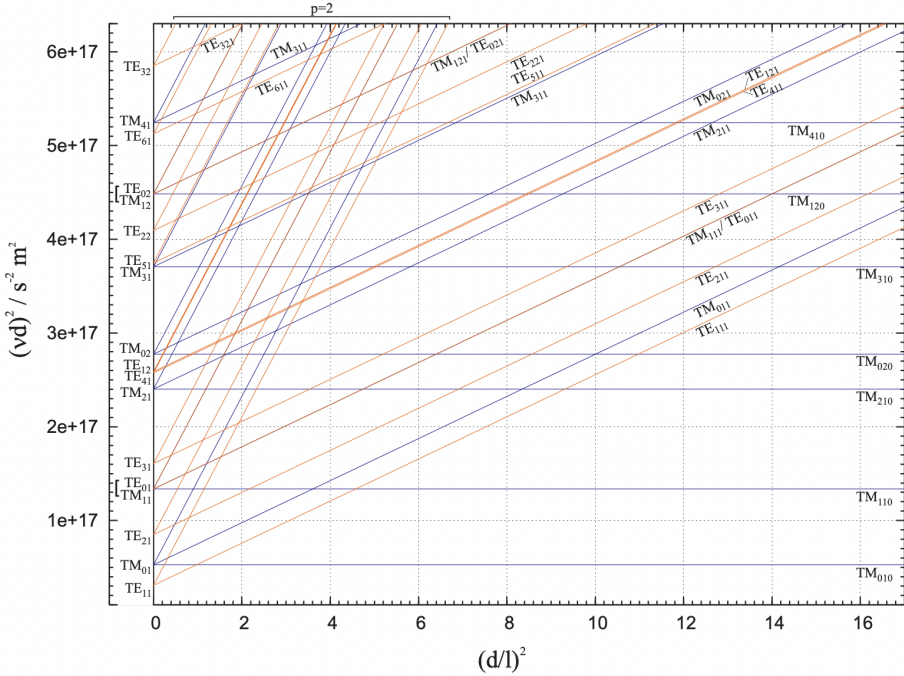


Figure 2.1.1: Mode map for $p \leq 2$. [3]

here d is the diameter of the cavity. When we plot different modes on a graph, we get a mode map (Fig.2.1.1). The mode map allows one to read off the resonant frequencies for different diameters and length of the cavity.

Since the derivative of the zeroth order Bessel function and the first order Bessel function, j'_{0n} and j_{1n} , are equal, the corresponding TE- and TM-modes have the same resonant frequencies. That is, TE_{0np} -modes and TM_{1np} -modes have the same resonant frequency.

2.2 Oscillating circuit

A cavity has a lot of characteristic quantities, which can be described by an equivalent circuit (Fig.2.2.1).

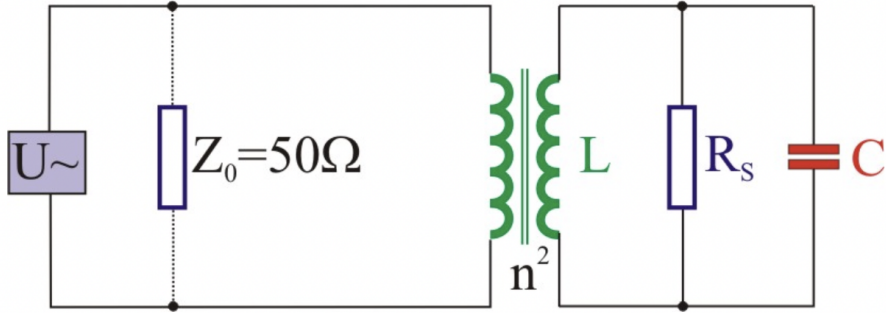


Figure 2.2.1: Equivalent circuit of a cavity with loop coupling. [3]

Coupling is a process through which electromagnetic waves can be coupled to a waveguide, or in this case, to a cavity. There are several ways to couple and in this experiment, we use loop coupling, which enables coupling to the magnetic field inside the cavity. In the figure 2.2.1, the LCR-circuit represents the cavity. The step-down transformer represents the loop coupling, Z_0 is the characteristic impedance and R_s is the Shunt impedance.

The characteristic quantities associated with the cavity are:

- Quality factor
- Coupling coefficient
- Reflection coefficient
- Shunt impedance

Let us look at these quantities in a bit more detail.

2.2.1 Quality factor

Quality factor is a dimensionless quantity which describes how underdamped an oscillator or resonator is. It is defined as:

$$Q_0 = \frac{2 \cdot \pi \text{ stored energy}}{\text{losses per period}} = \frac{2\pi \cdot W}{T \cdot P} = \frac{\omega_0 \cdot W}{P} \quad (2.2.1)$$

where ω_0 is the angular resonant frequency. Looking at the case of driven oscillations, the unloaded quality factor can be determined from the Full Width Half Maximum (FWHM), $\Delta\omega_H$

$$Q_0 = \frac{\omega_0}{\Delta\omega_H} \quad (2.2.2)$$

2.2.2 Coupling coefficient

The coupling coefficient is defined as:

$$\kappa = \frac{Z_a}{Z_0} = \frac{R_s}{n^2 Z_0} = \frac{Q_0}{Q_{ext}} \quad (2.2.3)$$

where n is the transformer turn ratio, Q_0 is the unloaded quality factor and Q_{ext} is the external quality factor. If we know the coupling coefficient, the unloaded quality factor can be calculated using:

$$\begin{aligned} \frac{1}{Q} &= \frac{1}{Q_0} + \frac{1}{Q_{ext}} \\ Q_0 &= (1 + \kappa) \cdot Q \end{aligned} \quad (2.2.4)$$

We also get 3 cases for the coupling coefficient, which are:

- $\kappa < 1$: undercritical coupling, $Q > Q_0/2$
- $\kappa = 1$: critical coupling, $Q = Q_0/2$ (no reflection)
- $\kappa > 1$: overcritical coupling, $Q < Q_0/2$

2.2.3 Reflection coefficient

In the conductor, we have an incoming wave (\hat{U}_+, \hat{I}_+) and reflected wave (\hat{U}_-, \hat{I}_-) . Hence we define the complex reflection coefficient as:

$$\rho = \frac{\hat{U}_-}{\hat{U}_+} \quad (2.2.5)$$

The coupling coefficient and the reflection coefficient are related at resonance by:

$$\kappa = \left| \frac{1 + \rho}{1 - \rho} \right| \quad (2.2.6)$$

We shall discuss more about this in the next section.

2.2.4 Shunt impedance

Shunt impedance tells us how much energy is gained by a charged particle when it crosses the cavity. It is defined by:

$$R_s = \frac{U^2}{2P_V} = \frac{1}{P_V} \left| \int_{L/2}^{-L/2} E_0(s) \cdot e^{i\omega_0 s/c} \cdot ds \right|^2 \quad (2.2.7)$$

The impedance of the resonator in fig.2.2.1 is a complex quantity. This value only becomes real at resonance and when it does, it is called the Shunt impedance. This value is typically of the order of $10^6 \Omega$. This is the reason we use a step down transformer in the circuit, using loop coupling, as seen in Eq.(2.2.3).

2.3 Scalar measurement of reflection coefficient

The reflection coefficient we defined in the previous section (eqn. 2.2.5) is a complex value. It looks like:

$$\rho(\Delta\omega) = \rho_0(\Delta\omega) \cdot e^{-2ikl} = \frac{\kappa - (1 + 2iQ_0 \frac{\Delta\omega}{\omega})}{\kappa + (1 + 2iQ_0 \frac{\Delta\omega}{\omega})} \cdot e^{-2ikl}$$

We get this when we investigate only take $\Delta\omega \ll \omega_0$. When this reflection coefficient is measured some distance l away from the cavity, we get the delay factor of e^{-2ikl} .

Now, we can separate the real and imaginary part and get its modulus:

$$|\rho(\Delta\omega)| = |\rho_0(\Delta\omega)| = \sqrt{\frac{(\kappa - 1)^2 + 4Q_0^2 (\Delta\omega/\omega)^2}{(\kappa + 1)^2 + 4Q_0^2 (\Delta\omega/\omega)^2}} \quad (2.3.1)$$

The scalar network analyzer should then look like fig. 2.3.1.

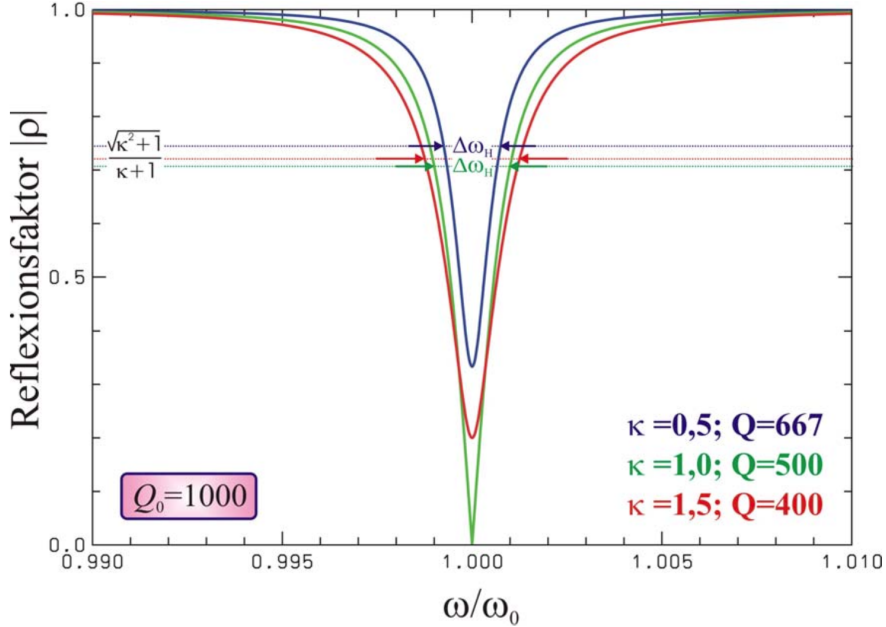


Figure 2.3.1: Reflection coefficient for different values of coupling coefficient and Quality factors along with FWHM ($\Delta\omega_H$). [3]

From the figure, we can see that the reflection is minimum at resonance. At resonance, the value of the reflection coefficient is given by:

$$|\rho(\Delta\omega = 0)| = \left| \frac{\kappa - 1}{\kappa + 1} \right| \quad (2.3.2)$$

The equation can be inverted to calculate the value of coupling coefficient as such:

$$\kappa = \begin{cases} \frac{1+|\rho|}{1-|\rho|} : & \rho > 0 \\ \frac{1-|\rho|}{1+|\rho|} : & \rho < 0 \end{cases} \quad (2.3.3)$$

As such, one cannot distinguish between $\rho > 0$ and $\rho < 0$.

In order to calculate the value of reflection coefficient at FWHM, we use the following relation (which one can derive by using eqn.(2.2.2), (2.2.4) and (2.3.1)):

$$|\rho(\Delta\omega_H/2)| = \frac{\sqrt{\kappa^2 + 1}}{\kappa + 1} \quad (2.3.4)$$

It is important to note that only the case of $\kappa = 1$ do we get the FWHM at $\rho = 1/\sqrt{2}$. This is because of the way we define dB-values, which will be discussed in another section.

In all other cases,

$$|\rho(\Delta\omega_H/2)| = \frac{\sqrt{\kappa^2 + 1}}{\kappa + 1} \neq \frac{1}{\sqrt{2}}$$

The (loaded) quality factor Q is then determined by following Eq. 2.2.2:

$$Q = \frac{\omega_0}{\Delta\omega_H} \quad (2.3.5)$$

The unloaded quality factor can easily be determined from Eq. 2.3.5 above:

$$Q_0 = (1 + \kappa)Q \quad (2.3.6)$$

2.4 Vectorial measurement of reflection coefficient

The vectorial reflection coefficient is given by:

$$\rho(\Delta\omega) = \frac{(\kappa - 1)^2 - 4Q_0^2(\Delta\omega/\omega)^2 - 4i\kappa Q_0 \Delta\omega/\omega}{(\kappa + 1)^2 + 4Q_0^2(\Delta\omega/\omega)^2} \cdot e^{-2ikl} \quad (2.4.1)$$

Neglecting the delay coefficient term, e^{-2ikl} , we get an equation, which when plotted on the complex plane (close to the resonance), ρ_0 describes a circle of radius r around (x_0, y_0) . The radius r is given by:

$$r = \frac{\kappa}{1 + \kappa}$$

We find that all the positions of circles are independent of quality factor and depend only on the coupling coefficient. Another interesting thing we find is that all these circles go through $(-1, 0)$ (as shown in fig. 2.4.1).

Now taking the delay coefficient into account, we see the circles rotate around the origin (fig. 2.4.2). For large values of quality factor, the distortion in the shape of the circle is negligible, but it is quite noticeable in low values of quality factor. We will be neglecting these distortions in our measurements because we such calibrations can be done only on expensive equipments.

In fig. 2.4.2, we also notice that we have an outer circle which is the reflection circle. It represents complete reflection of frequencies far away from the resonance one. The smaller circle is called the resonance circle.

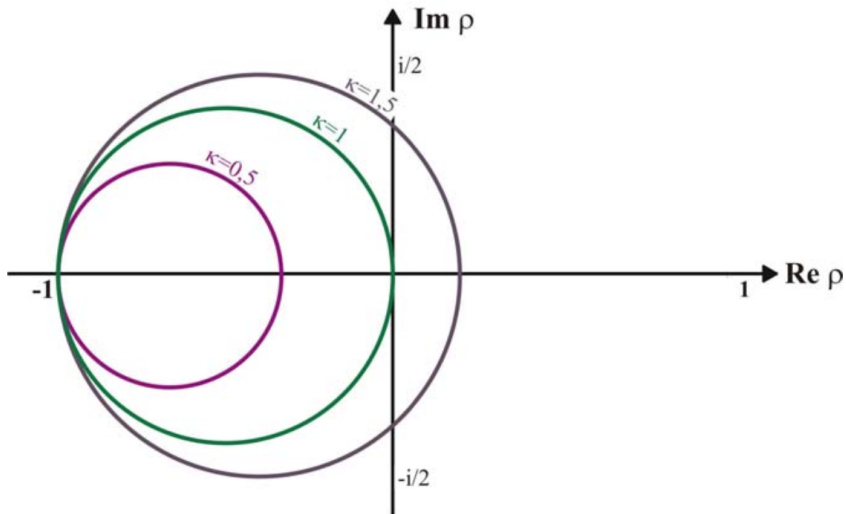


Figure 2.4.1: Different position and radii for different values of κ . [3]

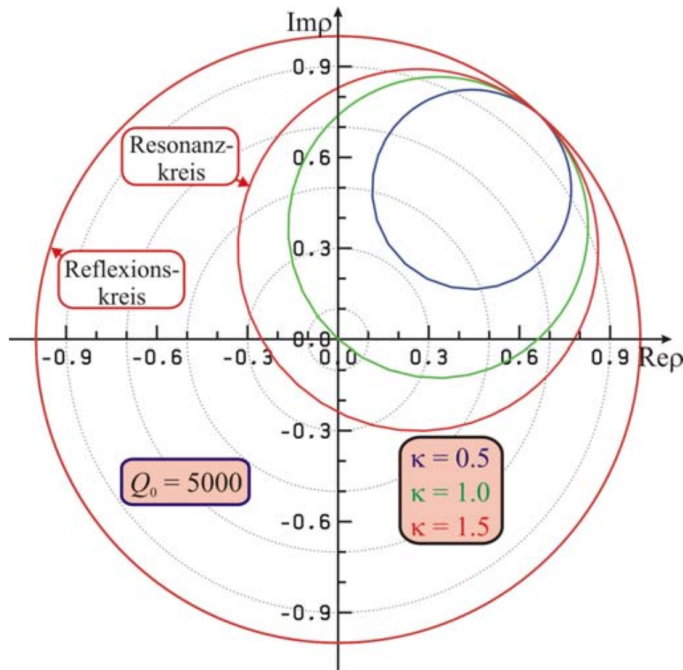


Figure 2.4.2: The delay coefficient rotates the circle around the origin. We can also see the Resonance and Reflection circle. [3]

2.4.1 Determining resonant frequency and coupling

In the Vectorial Network Analyzer (VNA), we see something similar to Fig. 2.4.2. In order to determine the reflection coefficient, we rotate the circles around the origin such that the point of intersection of the resonant circle and reflection circle is on $(-1, 0)$. Since the impedance of the resonator is real at resonance, the curve has to cross the real axis. Therefore, the point at which the resonance circle meets the real axis is the resonance frequency ω_0 .

In order to determine the reflection coefficient, we simply look at the distance between the resonant point and the origin, d , and the radius of the reflection circle, R . The reflection coefficient is then defined as:

$$\rho_0 = d/R$$

The coupling coefficient is given by:

$$\kappa = \frac{1 + \rho_0}{1 - \rho_0}$$

2.4.2 Determining quality factor

Similar to the scalar measurement, we use

$$\frac{\Delta\omega_H/2}{\omega_0} \approx \frac{1 + \kappa}{2Q_0}$$

and we get

$$\rho_0(\pm\Delta\omega_H/2) = -\frac{1}{\kappa+1} \mp i\frac{\kappa}{\kappa+1}$$

Therefore, the frequency shift $\Delta\omega$ from the resonant frequency and hence the FWHM can be determined by the intersection of the resonance circle around $(0, \pm i/2)$. This is essentially the frequency that is $\pi/2$ rotation away from the resonant frequency on the resonance circle.

2.5 Bead pull measurement

In order to measure the electric and magnetic field inside the cavity, we cannot use an antenna because that would disturb the field distribution inside. Instead, we introduce a small bead inside the cavity, a small perturbation. This bead, which is usually a dielectric or a conducting object, causes a shift in the resonant frequency, which can be measured. It can also be fixed with a constant excitation with ω_0 and the change in reflection coefficient can be observed. These two things can be used to determine the fields inside the cavity.

2.5.1 Resonant bead pull measurement

The case in which we measure the shift in the resonant frequency is called resonant bead pull measurement. A small teflon bead ($\epsilon_r = 2.1$, $r = 1\text{mm}$) is moved in small increments inside the cavity. For each increment, we get a shift in the resonance frequency $\Delta\omega(z)$. The Electric field, $E_0(z)$ is given by:

$$E_0(z) = \sqrt{2 \cdot \frac{W}{\alpha_S} \cdot \frac{\Delta\omega(z)}{\omega_0}} \quad (2.5.1)$$

where α_S is the perturbing constant:

$$\alpha_S = \frac{1}{2} \cdot (\epsilon - \epsilon_0) \cdot V_S$$

V_S is the volume of the bead.

2.5.2 Non-resonant bead pull measurement

The case in which we measure the change in reflection coefficient without changing the excitation is called non-resonant bead pull measurement. The electric field is determined by:

$$E_0(z) = \sqrt{\frac{(1 + \kappa)^2}{2\kappa Q_0} \cdot \frac{W}{\alpha_S} \cdot |\Delta\rho(z)|} \quad (2.5.2)$$

2.5.3 Shunt impedance

For determining the shunt impedance, it is sufficient to know the electric field. The accelerating voltage U is given by:

$$U = \int_0^L E_0(z) \cdot dz$$

Using this and Eqn. 2.2.7, we can define a delay coefficient as:

$$\Lambda = \left| \frac{\int_{-L/2}^{L/2} E_0(s) \cdot e^{i \frac{\omega_0 s}{c}} \cdot ds}{\int_{-L/2}^{L/2} E_0(s) \cdot ds} \right| \quad (2.5.3)$$

And finally, we have for resonant method:

$$R_s = \Lambda \cdot \frac{2Q_0}{\omega_0^2 \cdot \alpha_S} \cdot \left| \int_{-L/2}^{L/2} \sqrt{\Delta\omega(z)} \cdot dz \right|^2 \quad (2.5.4)$$

And for non-resonant method we have:

$$R_s = \Lambda \cdot \frac{(1 + \kappa)^2}{2\omega_0 \kappa \alpha_S} \cdot \left| \int_{-L/2}^{L/2} \sqrt{\Delta\rho(z)} \cdot dz \right|^2 \quad (2.5.5)$$

2.6 What is dB?

2.7 What is dBm?

2.8 Exercise before the experiment

Chapter 3

Experimental Setup

In our experiment, we used three cylindrical cavities, each with a length of $L_{cav} = 20$ mm with an inner diameter of $d_{cav} = 78.5$ mm. The first and second cavity are completely sealed and are free to move, but differ in their coupling position to the radio frequency. The third cavity is open from the sides and is mounted on a rail, in which its position can be freely adjusted and is displayed on an external device digitally. A thread with a teflon bead of radius $r_{bead} = 1$ mm and relative permittivity of $\epsilon_{r,bead} = 2.1$ was placed on the same mount such that the bead can pass through the cavity. The cavities used are shown in Fig. 3.0.1.

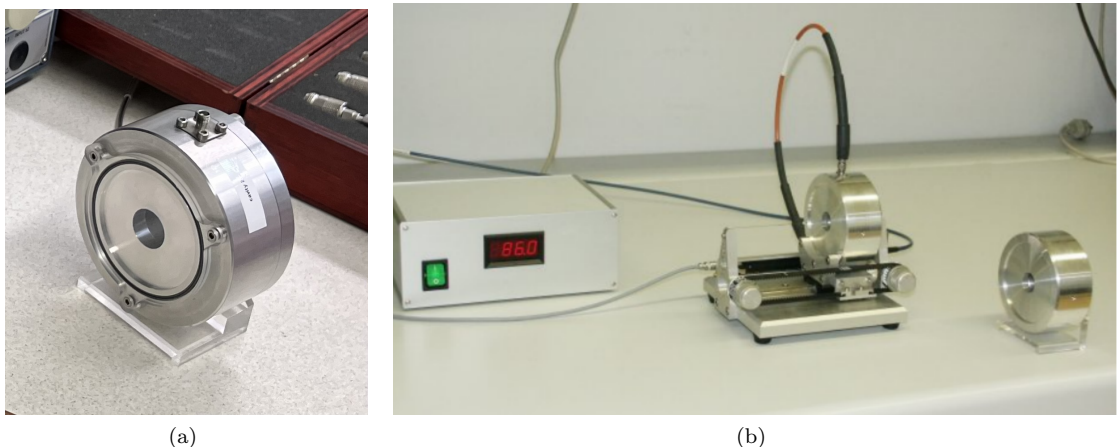


Figure 3.0.1: The three cavities used in this experiment. (a): The cavity with top coupling. The connector that couples the radio frequency can be observed. (b) The cavity with side coupling (right) and the mounted cavity (left) [5]. The detector used to measure the position of the mounted cavity is also shown.

To measure the resonant frequencies, reflection coefficients, and other relevant quantities in our experiment, we utilize a Vector Network Analyzer (VNA) shown in Fig. 3.0.2. The VNA generates a signal from its AC source and it is transmitted through the coaxial cable connected to the ports of the VNA. The resulting transmission or reflection of the signal is then shown on the display as a function of the frequency of the signal (in Hz). The units displayed can be altered between U , the ratio between output and input signal, and $dB = 20 \log_{10}(U)$.

3.1 Procedure

3.1.1 Attenuation and Reflection in Coaxial Cables

As the coaxial cable connects the cavity to the VNA, we need to choose a cable such that it does not interfere with the measurement of the cavity's response. To determine the optimal coaxial cable to use, we thus measured the attenuation and reflection of different coaxial cables at different frequency ranges. In our experiment, this was done for the RG-142 and ST-18 cables with a length of $l_{RG142} = 51.02 \pm 0.10$ cm

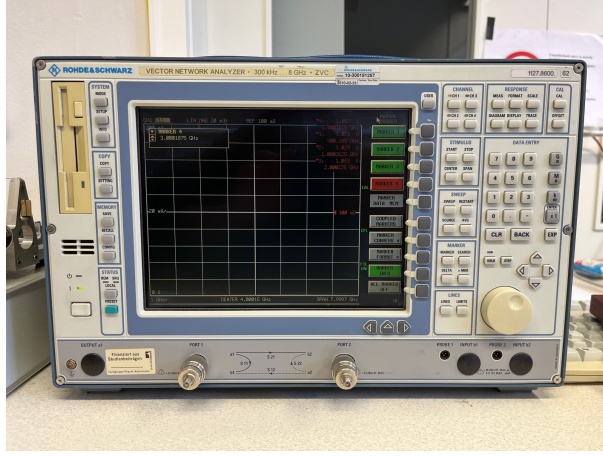


Figure 3.0.2: The Rhode & Schwarz Vector Network Analyzer used in this experiment.

and $l_{ST18} = 182.55 \pm 0.10$ cm respectively. The uncertainty of the length was obtained from the width of the scale of the measuring apparatus.

To measure the attenuation and reflection, we first calibrated the VNA to the silver RG402 coaxial cable with a length of $l_{RG402} = 30.02 \pm 0.01$ cm. The calibration process was performed using a full-two port calibration with the TOSM algorithm provided by the VNA. The open, short, and load (with termination impedance of 50Ω) at the two ports (port 2 on the VNA and the coaxial cable) were then calibrated by utilizing the provided calibration kit (Fig. 3.1.1).



Figure 3.1.1: The open (left), short (middle) and load (right) used for calibration in this experiment.

The attenuation of the signal was then measured by connecting the end of the coaxial cable to the input port (port 2) on the VNA. We then connect the same load from the calibration kit to the end of the coaxial cable to measure the reflection coefficient. Both measurements were performed to verify that the VNA was properly calibrated.

After the calibration was performed with the silver cable, we connected the two coaxial cables to the silver cable and measured their attenuation and reflection coefficient by performing the same procedure as with the silver one. The raw measurements obtained are shown in Fig. 3.1.2. The fluctuations in the signal were taken into account as the uncertainty in the coefficients. We neglected effects due to the connector between the two cables.

The transmission and reflection at several frequencies were then tabulated and were used to determine the attenuation of the cable. The attenuation λ (in units of dB m^{-1}) of a coaxial cable can be determined by the ratio of the reflected and transmitted power P_R , P_T as such:

$$\lambda = 20 \log_{10} \left(\frac{P_{in}}{P_{out}} \right) = 20 \log_{10} \left(\frac{P_R}{P_T} \right) \quad (3.1.1)$$

The resulting attenuation was then compared to those provided in the datasheets from the manufacturers.

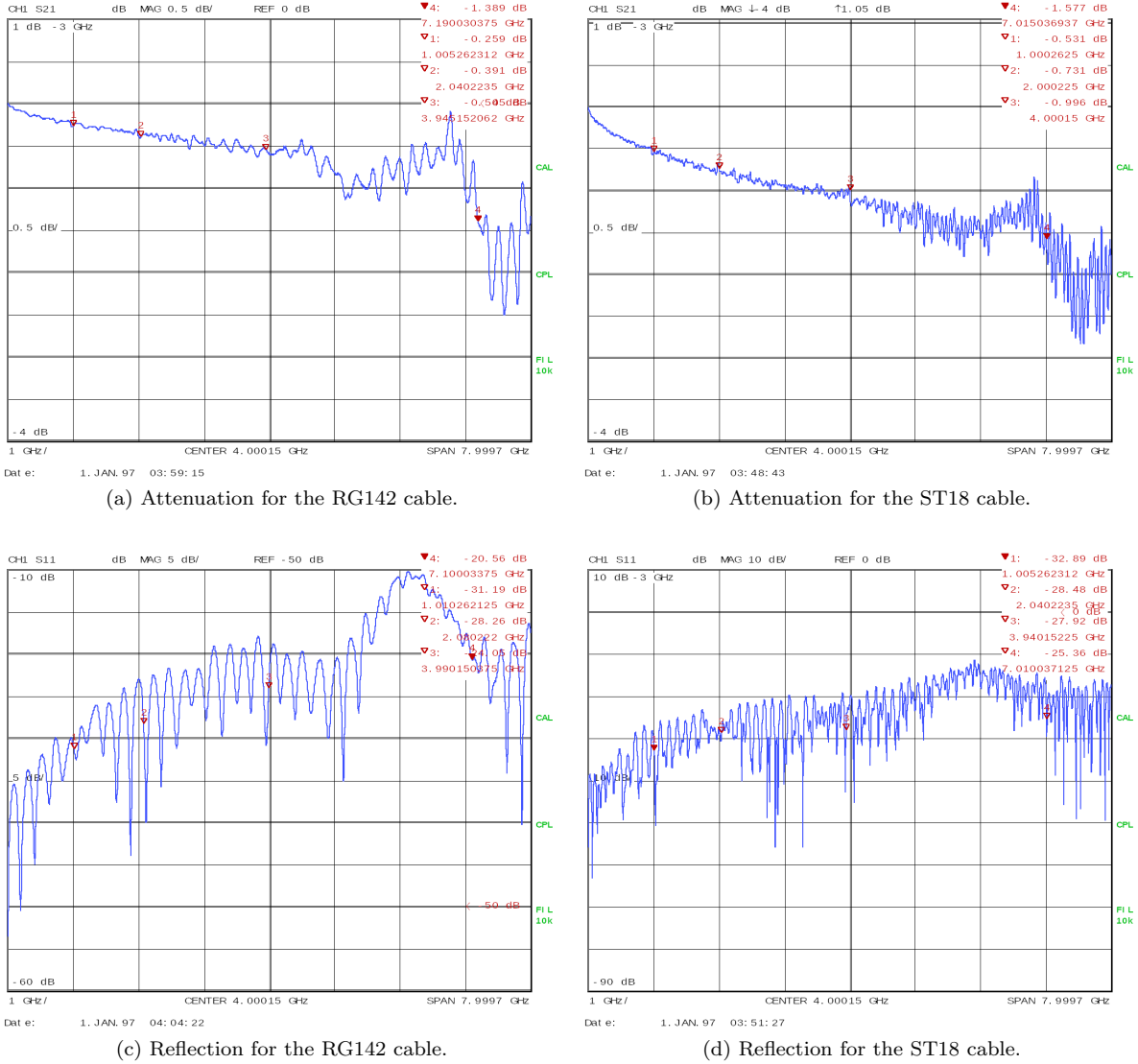


Figure 3.1.2: The attenuation and reflection for the RG142 and ST18 coaxial cables. The values at several frequencies are also shown on the top right of each figure.

3.1.2 Scalar Measurement

We then connected the brown coaxial cable to the top cavity (cavity with top coupling), and the resulting reflection coefficient was displayed on the VNA. We then pinpointed several points in frequency in which a sharp dip in the reflection curve was observed. Such points corresponded to resonant modes in the cavity. Before taking the measurement of each resonant frequency, the VNA was calibrated using a full one-port procedure, calibration with the kit from Fig. 3.1.1 as before. An example of a resonance in the reflection curve is shown in Fig. 3.1.3. The corresponding reflection coefficient and resonant frequency was then measured. The fluctuations and width of the scales taken into account as uncertainties in the reflection coefficient. The step size of the VNA was also considered as the uncertainty in frequency measurements.

To obtain the full-width half-maximum (FWHM) of the curve, the reflection coefficient obtained at resonance $|\rho(\omega_0)|$ was used to determine the coupling coefficient as shown in Eq. 2.3.3. The reflection coefficient at $\frac{\Delta\omega_H}{2}$ was then evaluated by using Eq. 2.3.4 and the corresponding frequency values were measured using the display. The loaded and unloaded quality factor was then determined using Eq. 2.3.5 and 2.3.6 respectively. Gaussian error propagation techniques were utilized to obtain the correct uncertainties for relevant quantities.

This procedure was performed for each observed resonance peak until 8 GHz, the maximal frequency

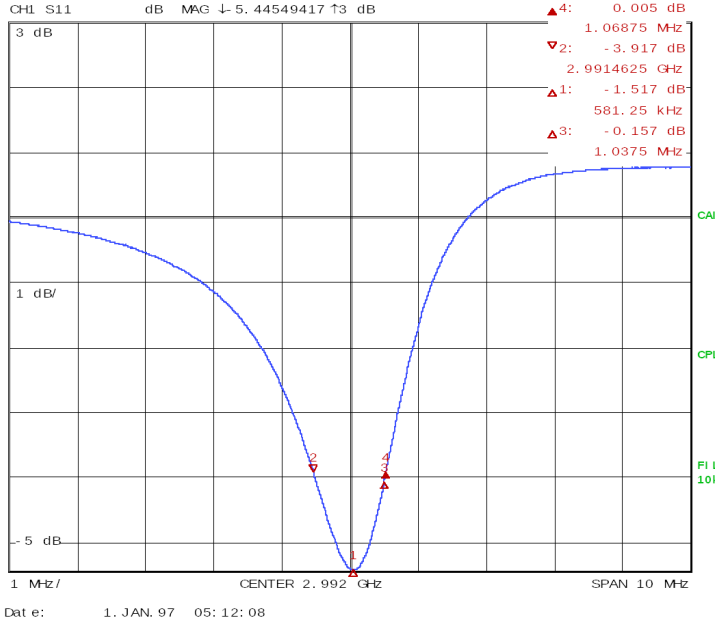


Figure 3.1.3: Reflection curve at a resonant frequency of $\omega_0 = 2.992\,206\,875$ GHz.

in which the VNA can measure. The same analysis was repeated for the side cavity, and the resonant frequency obtained in both cases were compared with the analytical resonant frequencies evaluated from Eq. 2.1.13.

3.1.3 Vectorial Measurement

We then used the top cavity to determine the resonant frequency and FWHM for the first fundamental eigenmode vectorially. This was done using the reflection curves as shown in Fig. 2.4.2, which is done by switching the display on the VNA to the complex representation.

The resonant frequency was first determined by using the same method as with the scalar analysis. We then switched to the complex representation and rotated the curve such that the point on the curve at resonance intersects with the real axis. The FWHM was then determined by first evaluating for the coupling coefficient, using the same equations as with the scalar analysis. The corresponding values of $|\rho(\frac{\Delta\omega_H}{2})|$ were then determined on the resonant circle, and the resulting frequency values were tabulated. The fluctuations of the measurement were again taken into account as uncertainties in our measurement. The obtained values were then used to determine the loaded, unloaded and external quality factor Q , Q_0 , Q_{ext} , as well as the power loss of the cavity. This was first performed without calibrating the VNA, and the same procedure was repeated after calibrating the VNA. The calibration was performed as with the scalar case. The results obtained from both cases were compared and discussed. A raw measurement of the resonant and reflection curves in both uncalibrated and calibrated cases are shown in Fig. 3.1.4.

3.1.4 Bead-Pull Measurement

We then connected the coaxial cable to the cavity mounted on the rail. Using the same method as with the scalar case, the location of the fundamental resonant mode was determined and the resonant frequency and FWHM was tabulated. These values were used to evaluate the quality factor Q , stored energy W , and the power loss of the cavity.

The cavity was then positioned such that the teflon bead was outside of the cavity. The position of the cavity was then adjusted, and using the scalar representation the change in resonant frequency $\Delta\omega_0$ and change in reflection coefficient at resonant frequency $|\Delta\rho(\omega_0)|$ were tabulated. The fluctuations and stepsize of the measurements were taken into account as the uncertainties in measurement. This was performed until the bead was completely outside of the cavity, which corresponds to a length of approximately 40 mm. The raw data can be observed in the Appendix section.

Using Eq. 2.5.1 and 2.5.2, the unperturbed electric field strength $E_0(z)$ was then determined for each position of the bead. Using the power loss obtained from above, we then evaluated the shunt impedance

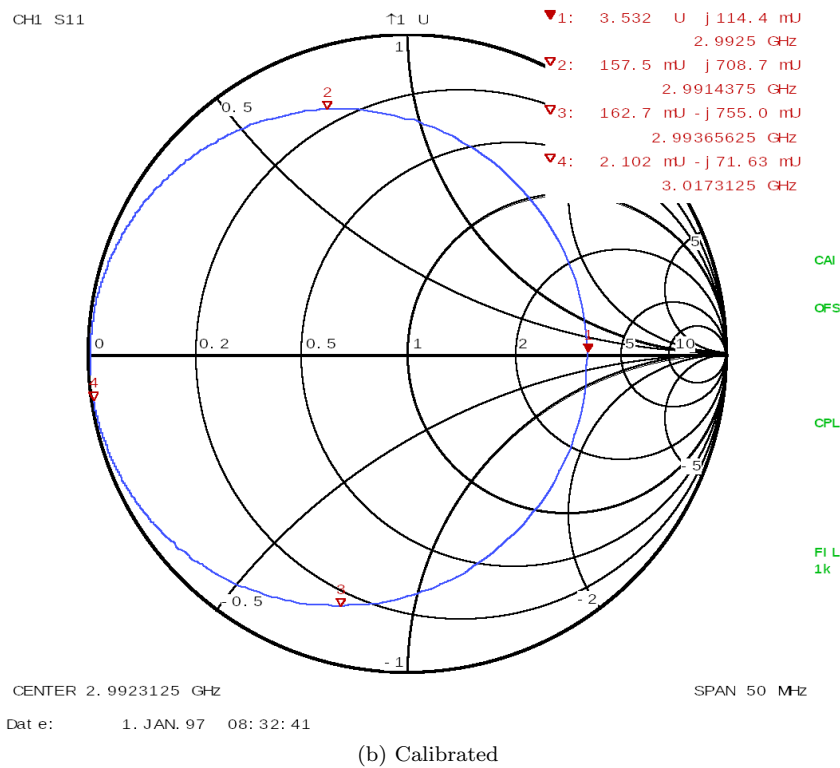
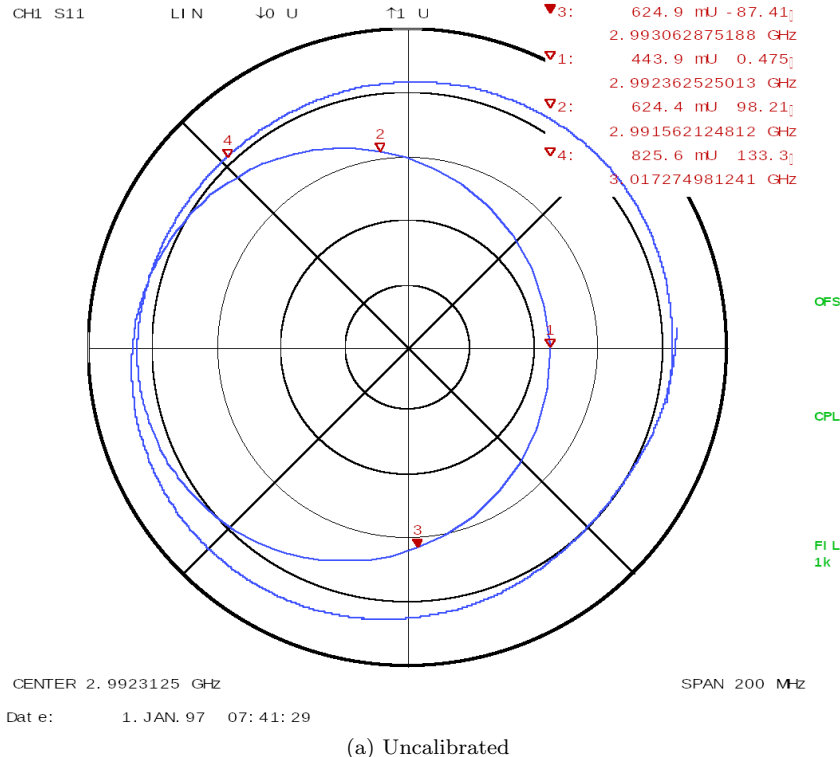


Figure 3.1.4: Vectorial measurement of the fundamental resonant mode (a) without and (b) with calibration. The curves are represented in linear polar and Smith representation respectively. The resonant frequency and points at half of the FWHM are indicated with markers 1, 2, 3 respectively.

R_s by utilizing cubic interpolations and Gauss-Legendre quadrature integration techniques. The transit time factor $\cos\left(\frac{\omega_0 z}{c}\right)$ was also taken into account when evaluating the shunt impedance, and the electric fields when considering such time factor was compared to those without this factor.

Finally, the energy gain of an accelerating particle was determined for several input powers. This was used to observe if our cavity was suited for particle accelerator experiments.

3.2 Results

3.2.1 Attenuation of Coaxial Cables

3.2.2 Scalar Measurement

Bibliography

- [1] W. C. Chew, *Lecture notes on ece 604 electromagnetic field theory*, Fall 2020.
- [2] W. Hillert, *Accelerator physics 1*, Summer 2006.
- [3] ——, *E106 hohlraumresonatoren / cavities: Details on the experimental method*.
- [4] D. J. Griffiths, “Electromagnetic waves,” in *Introduction to electrodynamics; 3rd ed.* Upper Saddle River, NJ: Prentice-Hall, 1999, ch. 9.
- [5] M. Switka, *E106 cavities assignments and details of procedure and analysis*, Mar. 2022.